LAWRENCE
LIVERMORE
NATIONAL
LABORATORY

LLNL-JRNL-663718

External Heat Transfer Coefficient Measurements on a Surrogate Indirect Inertial Confinement Fusion Target

R. Miles, M. Havstad, M. LeBlanc, I. Golosker, A. Chang, P. Rosso

November 5, 2014

Fusion Sciience and Technology ANS Publication

Disclaimer

EXTERNAL HEAT TRANSFER COEFFICIENT MEASUREMENTS ON A SURROGATE INDIRECT INERTIAL CONFINEMENT FUSION TARGET

Robin Miles, Engineer, Lawrence Livermore National Laboratory (LLNL)

Lawrence Livermore National Laboratory: P. O. Box 808, Livermore CA, 94551, miles7@llnl.gov

Mark Havstad, Engineer, LLNL

Mary LeBlanc, Engineer, LLNL

Ilya Golosker, Engineer, LLNL

Allan Chang, Engineer, LLNL

Paul Rosso, Engineer, LLNL

27 pages ; 2 tables; 15 figures

EXTERNAL HEAT TRANSFER COEFFICIENT MEASUREMENTS ON A SURROGATE INDIRECT INERTIAL CONFINEMENT FUSION TARGET

Robin Miles, Mark Havstad, Mary LeBlanc, Ilya Golosker, Allan Chang, Paul Rosso

Lawrence Livermore National Laboratory: P. O. Box 808, Livermore CA, 94551, miles7@llnl.gov

External heat transfer coefficients were measured around a surrogate Indirect inertial confinement fusion (ICF)based on the Laser Inertial Fusion Energy (LIFE) design target to validate thermal models of the LIFE target during flight through a fusion chamber. Results indicate that heat transfer coefficients for this target 25-50 W/m^2K are consistent with theoretically derived heat transfer coefficients and valid for use in calculation of target heating during flight through a fusion chamber.

Key words: inertial confinement fusion targets, thermal analysis, Laser Inertial Fusion Energy, LIFE

I. INTRODUCTION

Inertial confinement fusion (ICF) targets are typically designed to be injected into a fusion chamber [1-4]. The fusion chamber in the a Laser Inertial Fusion Energy (LIFE) concept design is filled with low-density xenon gas to minimize the heating of the chamber first wall by the post-implosion energized ions and gamma rays [5-7]. As a result, the chamber gas becomes very hot, ~6000K. The LIFE target must fly through this atmosphere on its way to the chamber center. This study investigates the convective heat transfer from the chamber gas to the target during the flight through the fusion chamber. The LIFE fusion chamber is on the order of 6m in diameter with flight velocities on the order of 250 m/s so the transit time is about 24 ms. The analytical studies for the heat transfer to the LIFE target in all phases of its flight are documented in Ref 8. Here, we perform experiments to begin to validate these results.

The candidate LIFE target is shown in Fig. 1 [7, 8]. The expected velocity profile around the target during flight through the fusion chamber, calculated using STAR-CCM [9], is shown in Fig. 2. The velocity profile is used to calculate a heat transfer coefficient following the Belov and Terpigor'ev correlation [10], simplified for use here takes the form:

$$Nu = \frac{hD}{k} = CRe^{n(Re)}Pr^{n(Pr)} \qquad \text{(Equation 1)}$$

The symbols are: Nu is the Nusselt number, h is the heat transfer coefficient, k is the thermal conductivity of the gas, D is the object diameter, C and n are constants, Re is the Reynold's number, Pr is the Prandlt number. Other works [11-14] have similar forms of this equation with differing values for the exponents. We validate the values for this heat transfer coefficient by flowing ambient gas over a pre-heated surrogate target and measuring the transient temperature differential between the gas and the target. The heat transfer coefficient was calculated based on the transient heat transfer equation:

$$\rho_{bd} C_{bd} V_{bd} \frac{dT_{bd}}{dt} = h(T_\infty - T_{bd}) A_{bd} - k_c (T_{bd} - T_m) A_c / \Delta x \qquad \text{(Equation 2)}$$

Here bd can denote the test target body. The variables are: ρ Is density , C is thermal capacity, V is the body volume, T is the temperature, t is time, h is the heat transfer coefficient, A is the area over which the heat flux is applied, k is the thermal conductivity of the target and x is the thickness. The subscripts are ∞ for the mid-air stream, c for the target attributes and m for the target interior. The conduction term on the right can represent the conductive heat loss to the interior of the surrogate target.

II. EXPERIMENTAL PROCEDURE

The test was conducted using a flow of gas through a pipe into which a surrogate target with external dimensions similar to the actual LIFE target was placed as shown in the diagram of Fig. 3. The target was pre-heated to temperatures of about 865 K then ambient air was drawn over the surrogate target and the heat transfer coefficient was calculated using Eq. 2 using the measured difference in temperature between the gas temperature and the surface temperature of the target.

A photograph of the external view of the test set-up is shown in Fig. 4. The surrogate test target is comprised of a hollow macor ceramic shell with holes drilled to permit the insertion of thermocouples through the interior core, through the drilled holes and mounted flush with the shell surface as shown in Figs. 5-7. Thermocouples used to measure the gas temperature were held with a supporting rod as shown in Figures 5 and 6. A clam-shell heater was wrapped around the flow tube into which the surrogate target was placed and was used to heat the apparatus to its initial temperature of about 865K prior to the gas flow. A vacuum pump pulled ambient air through the critical orifice located at the inlet

of the flow tube. Since the flow was choked as it traversed the critical orifice, the flow rate was dependent on the upstream pressure, in this case, atmospheric pressure. The flow rate through the flow tube was measured by the Bernoulli's differential pressure technique between the static and dynamic pressures. The gas pressure was about 23 torr and the gas velocity was about 25 m/s.

III. ANALYSIS AND RESULTS

STAR-CCM [9] simulations of flow around the test body at expected test conditions shown in Fig. 8 correlate well to that shown for target in flight through a fusion chamber. Both Figs. 2 and 8 show the higher acceleration in of the gas around the front corners of the target body where we expect high heat transfer coefficients. The frontal stagnation zones are similar between the test and expected actual fusion targets. The flow fields outside the cylindrical body portion of the target are also well matched. The necessity to remove instrumentation wires out the back end of the surrogate target assembly made the rear of the flow field different in the test case than in the case of flight through the fusion chamber so data near this area is not obtained.

Of particular interest is the transient response of the target shell for flight through the fusion chamber versus the test. Fig. 9 shows thermal profiles in the test body shell after 15 seconds of exposure to convective heating as expected in test. The small gradients in the test body shell suggest that data reduction assuming negligible thermal gradients locally in the test shell is adequate.

Test and expected fusion chamber use heat transfer coefficients and other conditions for the stagnation point are compared in Table 1. While the test conditions differ from the planned fusion chamber conditions, the measured heat transfer coefficients are comparable.

The heat transfer coefficient can be calculated using the constants of Eq. 1 found in the other cited works [10-13] as shown in Table 2, where the fluid properties have been evaluated at the "film" values, the average of the surface and free stream temperatures. The range of possible heat transfer coefficients is shown in the far right-hand column. Thus, for test conditions we expect heat transfer coefficients to vary from 25 to 40 W/m^2K.

The measured heat transfer coefficient results derived from the thermocouple data at three positions on the target; the stagnation point, front corner and mid-point on the side plotted as a function of time are shown in Figs. 10 through 15 for two separate tests (labeled A and B).

For all the plots the first few data points show very high scatter and should be considered unreliable. However the majority of the data around the peaks of the curves is very good and the results are consistent with both CFD modeling and the correlations described above. We expect that after two to four seconds of testing local conductive effects to the thermocouple wires and the target shell support structure are becoming more significant relative to the thermal inertia effects quantified in the transient heat transfer equation given above. The dependence of the test results on thermocouple location is mostly as anticipated from the analysis. There is a high convection coefficient at the stagnation point, a significantly higher convection coefficient is observed at the corner point and lastly, a lower convection coefficient is observed down the cylindrical side of the target.

IV. CONCLUSION

The magnitude of the external heat transfer coefficients is largely consistent between the analysis and the test results suggesting that using heat transfer coefficients in the range of 25-50 W/m^2K for the LIFE targets are reasonable. The test results shown here validate the target flow and external heat transfer modeling performed in support of LIFE target design [8]. Further work can be conducted to measure the external heat transfer coefficient for target designs incorporating a recessed front end which can be used to reduce the heat transfer coefficient at the LEH window. This option is discussed in Ref. 8.

ACKNOWLEDGMENTS

This work was performed under the auspices of the U.S. Department of Energy by Lawrence Livermore National Laboratory under Contract DE-AC52-07NA27344. Lawrence Livermore National Security, LLC.

REFERENCES

1. W. R. MEIER et. al., "OSIRIS and SOMBRERO Inertial Confinement Fusion Power Plant Designs: Volume 1 Executive Summary and Overview," WSJA-92-01, DOE/ER/54100-1 (1992).
2. J. D. SETHAN et. al., "Fusion Energy with Lasers, Direct-drive Targets, and Dry Wall Chambers," *Nuclear Fusion*, **43**, 1693 (2003).
3. R. W. PETZOLDT, "Inertial Fusion Energy Target Injection, Tracking and Beam Pointing," PhD Thesis, LLNL UCRL-LR_120192; UC-7712 (1995).
4. T. NORIMATSU et. al., "Influence of Gases on Direct-drive Cryogenic Targets in Laser Fusion Reactor with Wet Wall," *Fusion Engineering and Design*, **65**, 393 (2003).
5. M. Dunne et. al. "Timely Delivery of Laser Inertial Fusion Energy (LIFE)", *Fusion Science and Technology,* **60**, 19 (2011).

6. J. F. LATKOWSKI, et. al., “Chamber Design for the Laser Inertial Fusion-based Energy (LIFE) Engine,” *Fusion Science and Technology,* **60**, 54 (2011).
7. R. MILES, et. al,. “Challenges Surrounding the Injection and Arrival of Targets at LIFE Fusion Chamber Center,” *Fusion Science and Technology,* **60**, 61 (2011).
8. R. MILES, et. al. “Thermal and Structural Issues of Target Injection into a Laser-Driven Inertial Fusion Energy Chamber”, *Fusion Science and Technology,* **66**, 343 (2014).
9. http://www.cd-adapco.com/products/star-ccm
10. I.A. BELOV and V.S. TERPIGOR’EV, *Inzhenerno-Fizicheskii Zhurnal*, **17.6**, 1106 (1969).
11. H. H. SOGIN, “A Summary of Experiments on Local Heat Transfer from the Rear of Bluff Obstacles to a Low Speed Airstream,” *Transactions of the ASME: Journal of Heat Transfer,* **86** 200 (1964).
12. HADAD et.al. “Laminar Forced Convection Heat Transfer from Isothermal Bodies with Unit Aspect Ratio,” Paper presented at the 6th IASME/WSEAS International Conference on Heat Transfer, Thermal Engineering, and Environment, Rhodes, Greece (2008).
13. S. S. KANG and E. M. SPARROW. “Heat Transfer from an Open- or Closed- Bore Cylinder Situated Longitudinal to a Freestream,” *Transactions of the ASME: Journal of Heat Transfer,* **109** 314 (1987).
14. T.Y. NA and I. POP, “Flow and heat transfer over a longitudinal circular cylinder moving in parallel or reversely to a free stream,” *Acta Mechanica*, **118** 185 (1996).

Fig 1

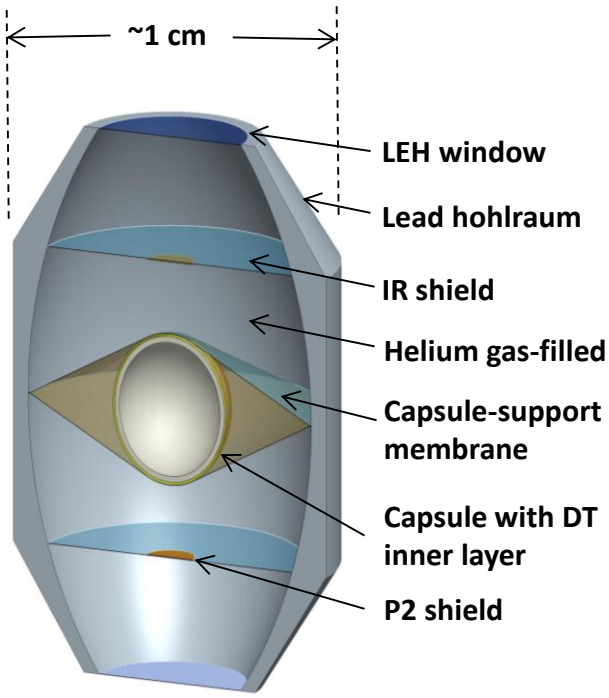
~1 cm
LEH window
Lead hohlraum
IR shield
Helium gas-filled
Capsule-support membrane
Capsule with DT inner layer
P2 shield

Fig 2

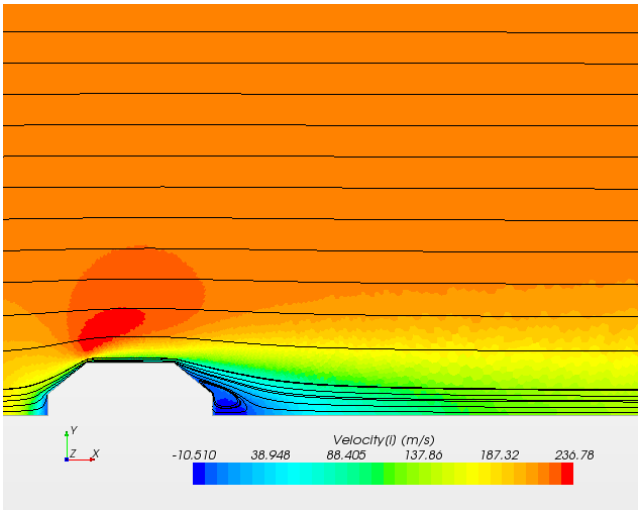

Fig 3

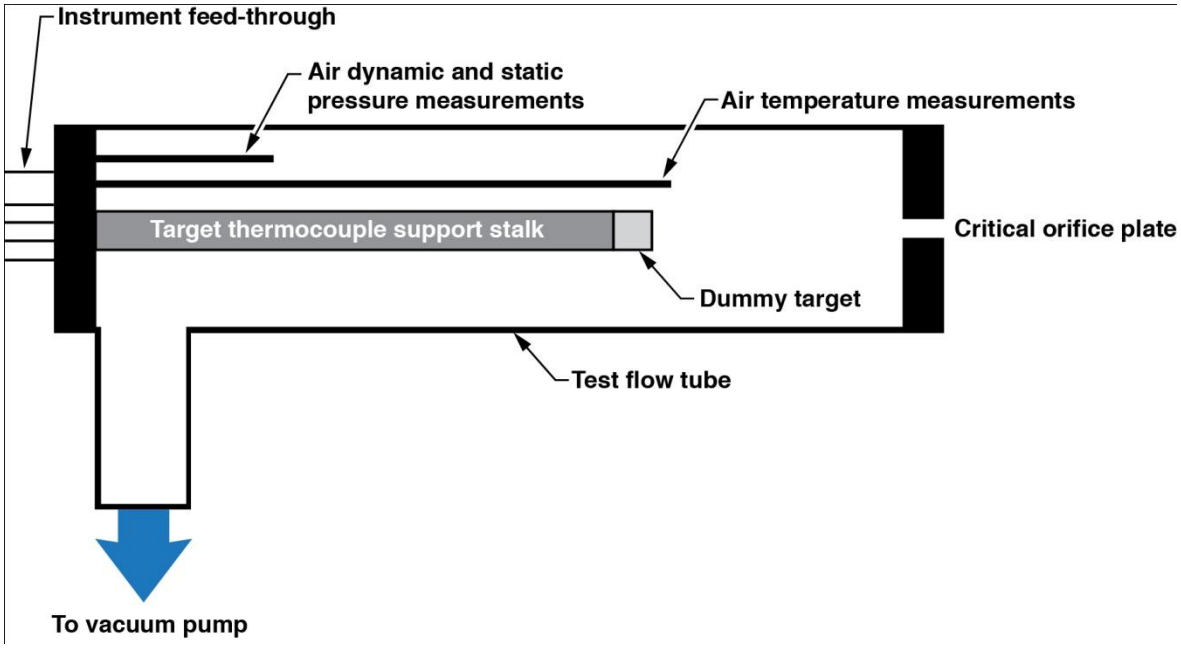
Instrument feed-through
Air dynamic and static pressure measurements
Air temperature measurements
Target thermocouple support stalk
Critical orifice plate
Dummy target
Test flow tube
To vacuum pump

Fig. 4

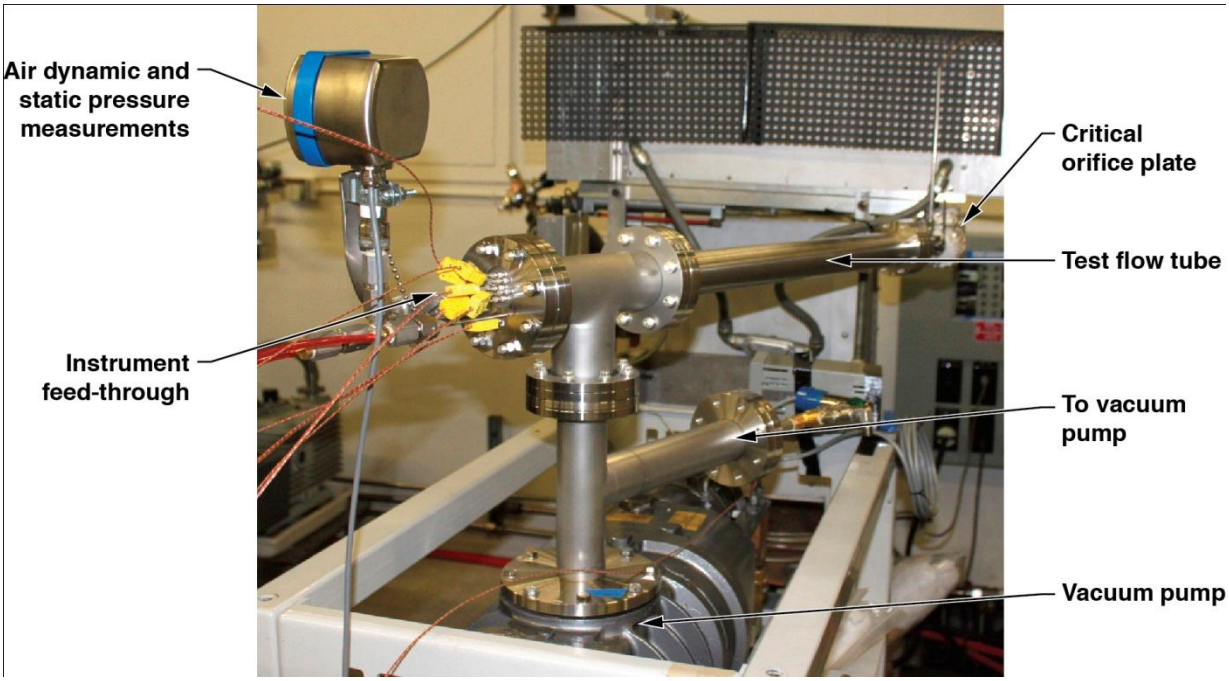
Air dynamic and static pressure measurements
Instrument feed-through
Critical orifice plate
Test flow tube
To vacuum pump
Vacuum pump

Fig 5.

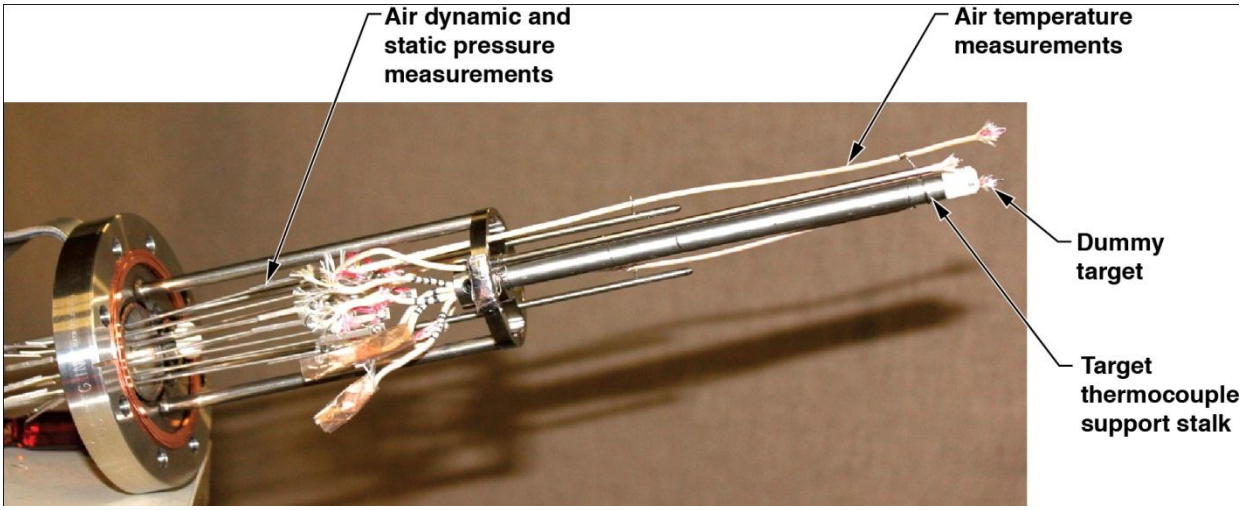
Air dynamic and
static pressure
measurements
Air temperature
measurements
Dummy
target
Target
thermocouple
support stalk

Fig 6

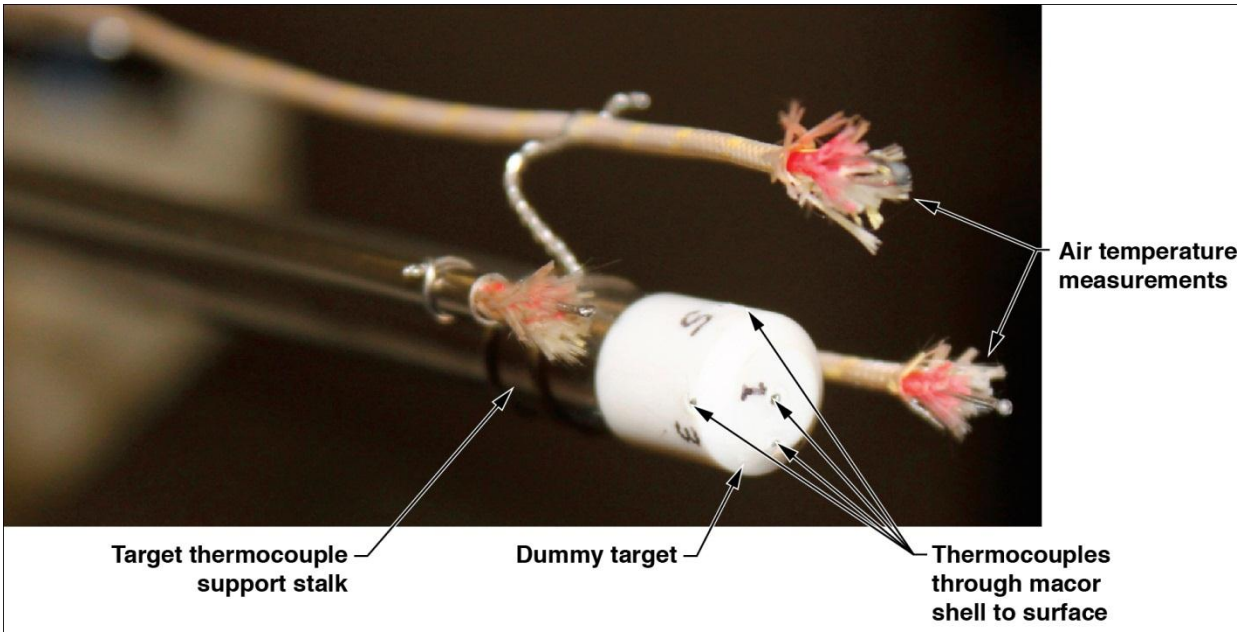
Air temperature measurements
Target thermocouple support stalk
Dummy target
Thermocouples through macor shell to surface

Fig 7

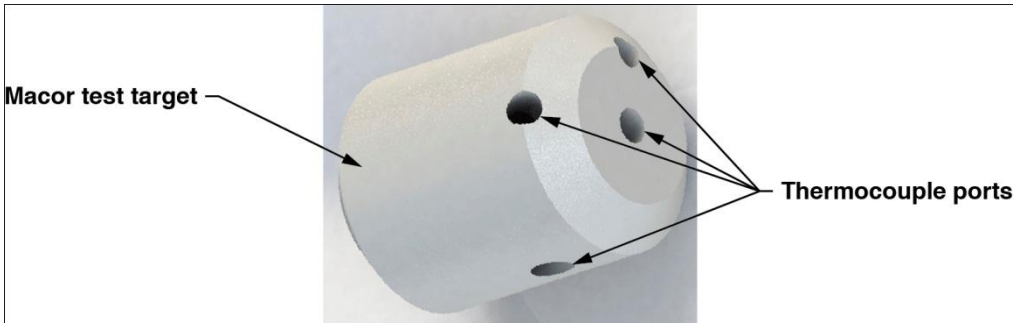

Fig 8.

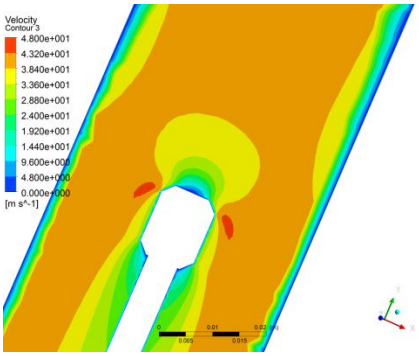
Velocity
Contour 3
4.800e+001
4.320e+001
3.840e+001
3.360e+001
2.880e+001
2.400e+001
1.920e+001
1.440e+001
9.600e+000
4.800e+000
0.000e+000
[m s^-1]

Fig 9.

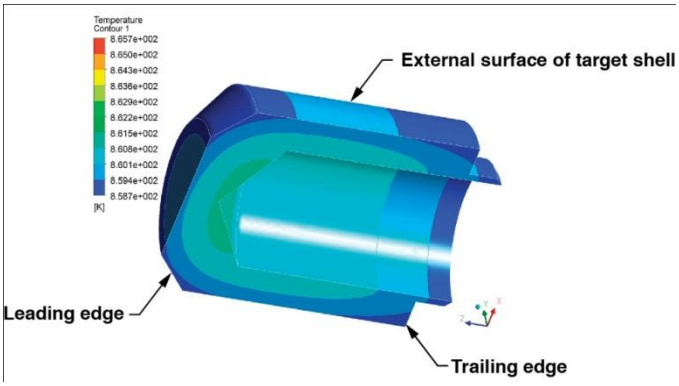
Temperature
Contour 1
8.657e+002
8.650e+002
8.643e+002
8.636e+002
8.629e+002
8.622e+002
8.615e+002
8.608e+002
8.601e+002
8.594e+002
8.587e+002
[K]
External surface of target shell
Leading edge
Trailing edge

Fig 10.

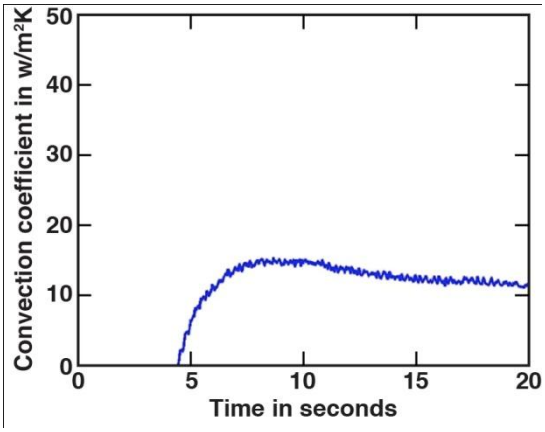
Convection coefficient in w/m²K
50
40
30
20
10
0
0
5
10
15
20
Time in seconds

Fig 11

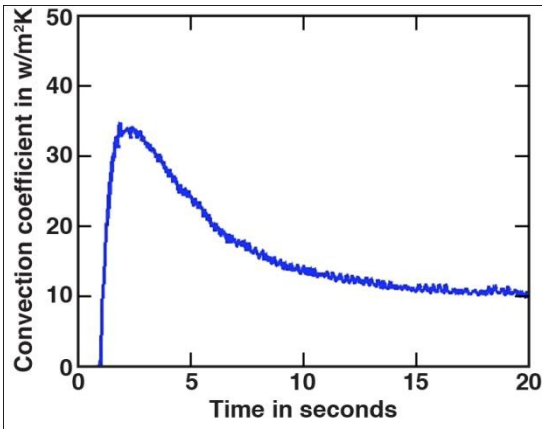
Convection coefficient in w/m²K
50
40
30
20
10
0
0
5
10
15
20
Time in seconds

Fig 12

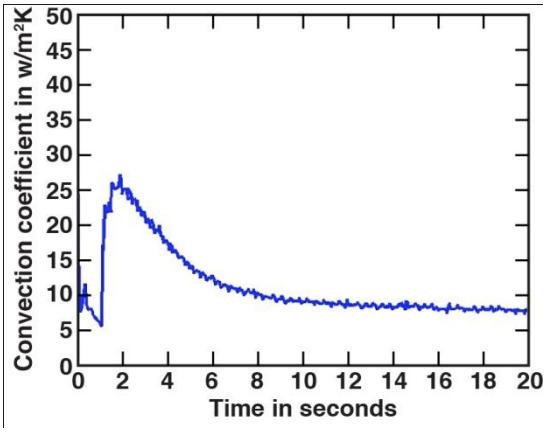
Convection coefficient in w/m²K
50
45
40
35
30
25
20
15
10
5
0
0
2
4
6
8
10
12
14
16
18
20
Time in seconds

Fig 13

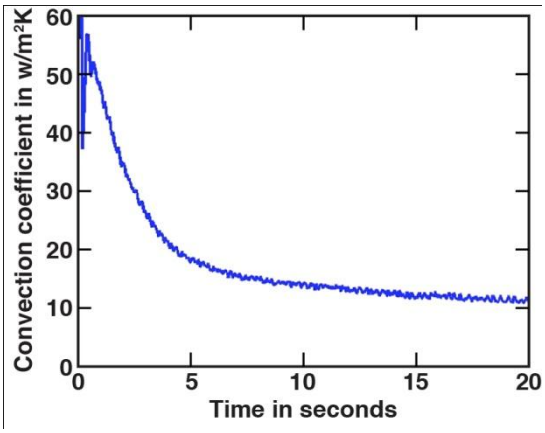
Convection coefficient in w/m²K
60
50
40
30
20
10
0
0
5
10
15
20
Time in seconds

Fig 14

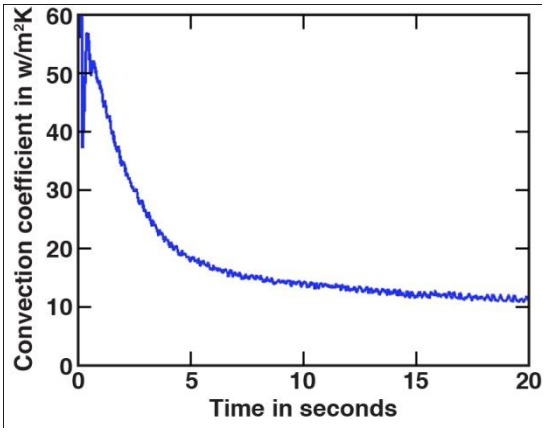
Convection coefficient in w/m²K
60
50
40
30
20
10
0
0
5
10
15
20
Time in seconds

Fig 15

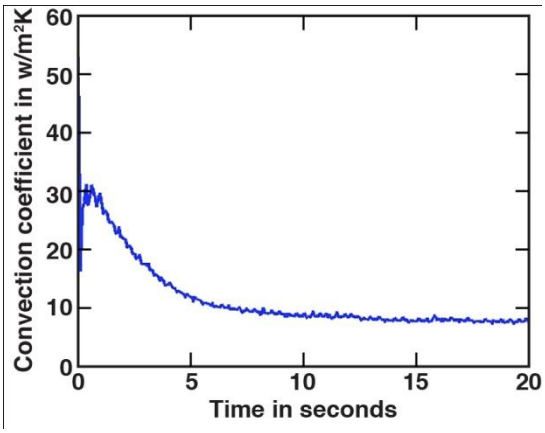
Convection coefficient in w/m²K
60
50
40
30
20
10
0
0
5
10
15
20
Time in seconds

Table 1

Parameter	Fusion chamber use	Test Condition	Units
Surface temperature	20	800	K
Gas temperature	6000	800	K
Gas pressure	3040	4400	Pa
Gas molecular weight	131	29	Kg/kmol
Prandtl number	0.8	0.76	
Reynolds number	280	270	
Nusselt number	12	9	
Heat transfer coefficient	31	40	W/m^2K
Mach number	0.31	0.044	

Table 2

Reference	C	n(Re)	n(Pr)	NuFilm	h (W/m^2K)
Belov	0.76	0.50	0.40	9.04	39.54
Sogin	0.20	0.67	0.00	6.37	27.88
Hadad	0.81	0.50	0.33	18.36	34.73
Kang	0.20	0.67	0.33	5.79	25.34